Spin relaxation in alkali-metal $^1\Sigma_g^+$ dimers

S. Kadlecek,[1] L. W. Anderson,[1] C. J. Erickson,[2] and T. G. Walker[1]
[1]*Department of Physics, University of Wisconsin-Madison, Madison, Wisconsin 53706*
[2]*Joseph Henry Laboratory, Physics Department, Princeton University, Princeton, New Jersey 08544*
(Received 7 May 2001; published 15 October 2001)

We discuss the relaxation of a spin-polarized alkali-metal vapor due to the electric-quadrupole interaction in $^1\Sigma_g^+$ dimers, and present a model that accurately describes the measured relaxation rates under a wide variety of conditions. We use the model along with experimental results to deduce the quadrupole interaction strength, atom-dimer chemical-exchange reaction rate, and the rate of reorientation of singlet dimers due to collisions with the buffer gas.

DOI: 10.1103/PhysRevA.64.052717 PACS number(s): 32.80.Cy, 32.80.Bx, 33.35.+r

I. INTRODUCTION

Spin-polarized noble gases [1,2] have important applications in such diverse areas as magnetic-resonance imaging [3], precision measurements with audio-frequency masers [4], neutron-spin filters [5], targets for high-energy electron-scattering experiments [6], and surface and diffusion studies [7–10]. The noble-gas nuclei are typically polarized through spin-exchange collisions with an electron-spin-polarized alkali-metal vapor. Since the efficiency of this process is limited by alkali-metal spin relaxation [2,11], a thorough understanding of alkali spin-relaxation processes is a topic of considerable importance. In this paper, we present studies of atomic Rb spin relaxation-due to the electric-quadrupole interaction in $^1\Sigma_g^+$ dimers.

Spin relaxation in alkali-metal vapors remains a complex and incompletely understood process, but a number of different mechanisms have been identified and studied. In order to put this work into perspective, Fig. 1 summarizes our measured Rb relaxation rates under a wide range of experimental conditions [12]. We see that, depending on alkali-metal density and buffer-gas pressure, relaxation may arise from collisions with the buffer gas [13], alkali-metal–alkali-metal interactions [11,14–18], diffusion to the container walls [13] or, at large alkali-metal density and low buffer-gas pressure, relaxation in singlet dimers. Other mechanisms, such as diffusion through magnetic-field gradients [13] and the formation of alkali-metal–buffer-gas van der Waals's molecules [19] are too small to be significant in our experiment.

Electric-quadrupole-relaxation studies in alkali-metal dimers were pioneered by Gupta *et al.* [20], who detected the nuclear magnetic resonance (NMR) signals from $^1\Sigma_g^+$ dimers in optically pumped Cs and Rb vapors. They found that the NMR linewidth depended on the molecular breakup rate, the chemical-exchange rate, and the rapid reorientation of the electric-quadrupole hyperfine interaction due to buffer-gas collisions. They found large chemical-exchange cross sections of the order of 100 Å^2, and cross sections for reorientation of the rotational angular momentum **J** of a few Å^2. The large chemical-exchange cross sections are consistent with detailed molecular-beam studies of atom-dimer-scattering cross sections. The NMR method was extended to Na [21,22], K [23], repeated for Cs [24], and used to study the small nuclear spin-rotation coupling in K_2 and Rb_2 [25].

In addition to determining the linewidth of dimer NMR signals, electric-quadrupole relaxation is also an important contributor to the spin relaxation of optically pumped alkali-metal atoms, though up to now no systematic studies have been done. In this work, by measuring spin-relaxation rates over a broad range of alkali-metal vapor density, buffer-gas pressure, and magnetic field, we deduce accurate values for the key parameters that govern spin relaxation in singlet dimers. Thus, we find that the Rb atom-dimer chemical-exchange cross-section is 173 ± 35 Å^2 and the root-mean-square electric-quadrupole interaction strength is $\Omega_Q/2\pi = 300\pm30$ kHz in a singlet dimer. We find that the cross section for a Rb singlet dimer to be reoriented by collisions

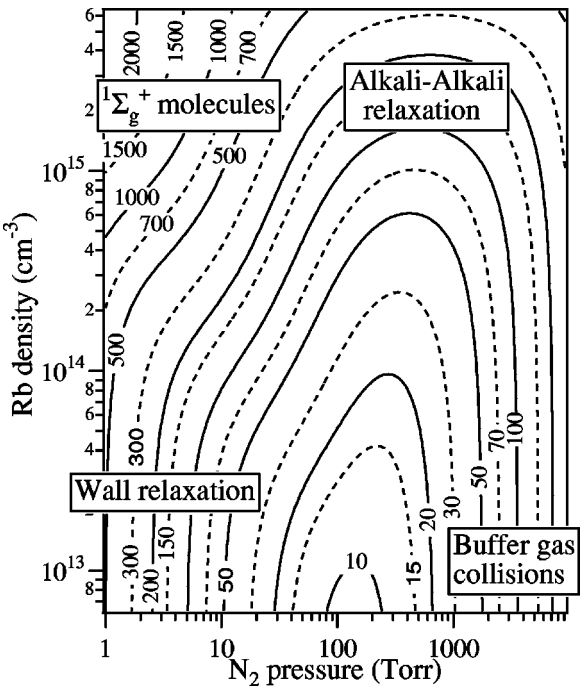

FIG. 1. Summary of measured relaxation rates for Rb in N_2 as a function of N_2 pressure and Rb density, for a long 1.5-in.-diameter cell. The contours shown are relaxation rate at low magnetic field in s^{-1}. The text inserts show the region of phase space in which each of the four relaxation mechanisms are dominant.

 ©2001 The American Physical Society

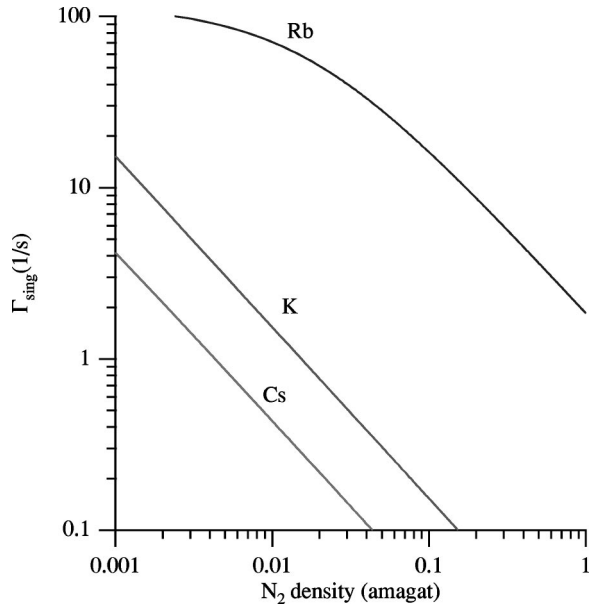

FIG. 2. Relaxation rates as a function of pressure due to quadrupolar and nuclear spin-rotation relaxation in alkali-metal singlet molecules, at an alkali density of 10^{14} cm^{-3}. The Rb line is calculated from the results of our experiments; the K and Cs lines are estimates based on the numbers given in Table I.

with N_2 is 12 ± 2 Å^2. All of these measurements were performed at temperatures near 500 K in vapors of natural isotopic Rb abundance. We present here a detailed analysis of quadrupolar relaxation that extends the work of Gupta *et al.* [20] and allows the relaxation rates to be calculated over a wide range of third-body pressures, Rb vapor pressures, and magnetic fields.

The results presented in the previous paragraph, and the bulk of the information to follow in this paper, were obtained from experiments at the University of Wisconsin, Madison. Extensive measurements and analysis of Rb spin relaxation due to singlet molecules have also been completed at Princeton University. This work will not be described in detail here, but the final experimental results will be presented. Further details are available in Ref. [26].

A detailed understanding of singlet relaxation was essential for our recent study of the spin-axis relaxation in alkali-metal triplet molecules [18]. It enabled us to separate out the singlet and triplet contributions to the relaxation rate for Rb, a step that was essential for successfully isolating the effects of spin-axis coupling in $^{87}Rb_2$ triplet molecules.

We emphasize in this paper the quadrupolar relaxation of Rb atoms. Because Cs has a small quadrupole moment, and K has a small electric field gradient, these atoms undergo negligible quadrupolar relaxation at typical spin-exchange optical-pumping densities of 10^{14} cm^{-3}. For Cs and K, the spin-rotation interaction is comparable strength to the quadrupole interaction. For these atoms, the total singlet-molecule relaxation, as compared to diffusion and other collisional processes, remains too small to make a significant contribution to spin relaxation under most conditions. Figure 2 shows the relaxation rates due to singlet molecules for the three atoms.

This paper is organized as follows. We begin in Sec. I with a discussion of the properties of alkali-metal singlet dimers that are essential to this paper, namely, the electric-quadrupole interaction and the exchange and breakup dynamics of singlet dimers in an alkali-metal-vapor/buffer-gas mixture. This leads to the model of relaxation in singlet dimers whose principal results are outlined in Sec. II, and discussed in more detail in appendices. Because our work is closely related to the previous NMR linewidth experiments, in Sec. III we discuss the NMR linewidth in the context of our model. Our experiments are described in Sec. IV, followed by comparisons to other work in Sec. V.

II. PROPERTIES OF ALKALI-METAL SINGLET DIMERS

A. Dimer density

At alkali-metal densities suitable for most applications of spin-polarized alkali-metal vapors (10^{14}–10^{15} cm^{-3}), roughly 1% of the alkali atoms are in $^1\Sigma_g^+$ dimers, which makes them by far the dominant molecular species. Although the singlet dimer has no net electron spin, the nucleus is subject to depolarization via the electric-quadrupole interaction and, to a lesser extent, via the nuclear spin-rotation interaction. These interactions couple the nuclear spin to the dimer rotational angular momentum, to which polarization is lost in collisions. Free atoms are continually being associated into dimer molecules, where their nuclei relax. Upon disassociation from the molecule, either by collisional breakup or chemical exchange, the atomic electron and nuclear spins return to spin equilibrium with other free atoms via the hyperfine interaction and spin-exchange collisions. Thus rapid polarization transfer, plus the large density of singlet molecules, make nuclear depolarization an efficient means of spin relaxation despite the relatively small coupling typical of nuclear interactions.

In order to make quantitative relaxation-rate calculations, we need to know the singlet-dimer density. Given the difficulty of experimentally measuring this, we determine it from the atom density and a calculation of the chemical-equilibrium coefficient. Because this procedure depends sensitively on the molecular potential, we have attempted to construct the most accurate potential possible by starting with the *ab initio* calculations of Ref. [27], scaling them to agree with recent spectroscopic determinations of the dimer binding energies [28–30] and matching them to the well-studied long-range $1/R^6$ potentials of Refs. [31,32]. Table I gives a convenient parametrization of the resulting potentials for K, Rb, and Cs, as well as the most recent determinations of binding energy and C_6 coefficients.

We numerically determined the energy eigenstates of these potentials and from them determined the chemical-equilibrium coefficient as

$$^1k_{chem}=\frac{1}{8}\left[\frac{h^2}{\pi m k_B T}\right]^{3/2}\sum_i e^{-E_i/k_BT}(2J_i+1) \qquad (1)$$

in which m is the atomic mass, and E_i are J_i and the energy

TABLE I. Properties of $^1\Sigma_g^+$ molecules relevant to quadrupole relaxation. D_E shows the values of the experimentally determined binding energies, in Hartrees. eqQ/h is the quadrupole coupling strength, while Ω_Q [see Eq. (6)] gives a better relative measure of the relaxation caused by the quadrupole interaction for different molecules. The relative importance of relaxation due to quadrupole and spin-rotation interactions is given by comparison of the squares of $c'\sqrt{\langle J^2\rangle}$ and Ω_Q. The other entries parametrize the potential as $V(r)=c_0e^{-r/r_0}+c_1\exp[-\{(r-r_1)/r_2\}^2]-C_6[(1-e^{-r/r_3})/r]^6$, in atomic units, and the chemical-equilibrium coefficient in the form $\ln(^1k_{chem})=\Sigma a_nT^n$, where T is the vapor temperature in K and the units of $^1k_{chem}$ are cm^3.

	K	Rb	Cs
D_E	0.02028 [a]	0.01820 [b]	0.01630 [c]
eqQ/h	−158 kHz [d]	85:>−1100 kHz [d] 87:>−580 kHz [d]	230 kHz [d]
$\Omega_Q/2\pi$	29.7 kHz [d]	85:300 kHz [e] 87:290 kHz [e]	14.4 kHz [d]
c'	72 Hz [f]	250 Hz [f]	101 Hz [f]
$c'\sqrt{\langle J^2\rangle}$	5.5 kHz	30 kHz	16 kHz
C_6	3813 [g]	4550 [h]	6330 [g]
c_0	7.720	7.712	3.291
c_1	-0.1471	-0.0447	-0.3285
r_0	1.3579	1.3579	2.2000
r_1	-0.513	4.354	-0.800
r_2	6.707	4.979	7.597
r_3	2.4974	2.4974	2.9727
a_0	2.707	-4.6452	-7.9145
a_1	-0.1781	-0.1470	-0.1426
a_2	2.551×10^{-4}	2.003×10^{-4}	2.043×10^{-4}
a_3	-1.350×10^{-7}	-1.005×10^{-7}	-1.081×10^{-7}

[a]Reference [29].
[b]Reference [30].
[c]Reference [27].
[d]Reference [33].
[e]This work.
[f]Reference [25].
[g]Reference [31].
[h]Reference [32].

and rotational angular momentum of the ith energy eigenstate. Corrections for Fermi statistics of the nuclei in the homonuclear case are negligible. The density of singlet dimers $[^1A_2]$ of alkali-metal species A is then given by the law of mass action as

$$[^1A_2]=^1k_{chem}[A]^2. \tag{2}$$

Table I gives a parametrized fit to $^1k_{chem}(T)$ for K, Rb, and Cs over a 350–600 K temperature range. The accuracy of this assumed $^1k_{chem}$ depends critically on the accuracy of the binding energy. Since we have scaled to the very accurate recent measurements, we estimate that our deduced $^1k_{chem}$ should be accurate to better than 10%. For reference, scaling from the calculated *ab initio* trap depth to the experimental one changes $^1k_{chem}$ by 15%.

B. The quadrupole interaction

The electric-quadrupole interaction for a single nucleus of spin I in a rotating singlet molecule takes the form (originally due to Casimir and discussed in detail in Ref. [34], Sec. 6-2)

$$V_Q=-eqQ\frac{[3(\mathbf{I}\cdot\mathbf{J})^2+\frac{3}{2}(\mathbf{I}\cdot\mathbf{J})-I(I+1)J(J+1)}{2I(2I-1)(2J-1)(2J+3)}, \tag{3}$$

in which Q is the nuclear electric-quadrupole moment and $q=\langle JJ|\partial^2V/\partial z^2|JJ\rangle$ is the electric-field gradient at the nucleus in the stretched rotational state. Selected values of eqQ/h are given in Table I. A nuclear spin-rotation interaction of the form [22,35]

$$V_{SR}=c'(\mathbf{I}\cdot\mathbf{J}) \tag{4}$$

is also present. While it is much smaller than the quadrupole interaction for Rb (contributing at most a few percent to the relaxation), it is an important contributor to the relaxation for K and is slightly larger than the quadrupole interaction for Cs, as shown in Table I [22].

At temperatures suitable for this experiment, and for most uses of a polarized alkali-metal vapor, the average dimer rotational angular momentum J is greater than $100\hbar$. The first and third terms of V_Q are therefore dominant, allowing Eq. (3) to be simplified to

$$V_Q\approx\frac{\hbar\Omega_Q}{3I}\mathbf{I}\cdot(3\hat{\mathbf{J}}\hat{\mathbf{J}}-1)\cdot\mathbf{I}, \tag{5}$$

where

$$\Omega_Q=-\frac{3eqQ/\hbar}{8(2I-1)}. \tag{6}$$

We will see later that in the important high-pressure limit, the relaxation rate is proportional to $|\Omega_Q|^2$, multiplied by factors that are approximately independent of I. This makes Ω_Q a better relative measure of the comparitive importance of the quadrupole interaction in different molecules than the more traditional combination $eqQ/\hbar$. For example, the values of Ω_Q from Table I readily explain the progression seen in Fig. 2.

It is important to point out that the electric-field gradient q depends on the rovibrational state of the molecule. Under most experimental conditions where quadrupolar relaxation is important, the appropriate value of q for use in Eq. (6) is the root-mean-square value averaged over the thermal distribution of molecular states.

C. Dimer kinetics

As is known from NMR studies, several processes interrupt the coherent evolution of the nuclear spins under the influence of V_Q. Singlet dimers are formed and dissociated, undergo chemical exchange with free atoms, and, on a much shorter time scale, are reoriented by collisions with the buffer gas. Since the quadrupole interaction depends on the direc-

tion of molecular angular momentum **J**, such reorienting collisions also halt coherent evolution.

The singlet dimer binding energy $D_E \sim 0.5$ eV is much larger than $k_B T$, so only infrequently will buffer-gas collisions transfer sufficient energy to cause dissociation. Three-body breakup and formation occur only rarely, and previous work [36] is consistent with the requirement that each $^1\Sigma_g^+$ molecule undergo approximately $\exp(D_E/k_B T) \approx 10^4$ collisions before dissociating.

On the other hand, free alkali-metal atoms can be readily associated into singlet dimers through chemical-exchange processes of the form

$$A_1 + (A_2 A_3) \rightarrow (A_1 A_2) + A_3. \tag{7}$$

This rate exceeds the three-body formation rate when the alkali-metal density exceeds approximately 10^{-5} of the buffer-gas density. Chemical-exchange processes are particularly important for spin relaxation, since they replace partially relaxed nuclei from the molecule with new polarized nuclei from the initially free atom. There is no Boltzmann suppression of the chemical-exchange process because it does not need to overcome the large singlet binding energy. Hence the chemical-exchange cross section is comparable to the total gas kinetic cross section.

In order to completely describe the molecular dynamics of singlet dimers in a buffer gas, we need to include three-body formation and breakup, chemical exchange, and **J**-reorienting collisions. However, because the cross section for reorientation is so much larger than for three-body breakup, relaxation during a molecular lifetime is very small whenever the buffer-gas pressure is high enough so that three-body breakup is significant. In this high-pressure regime, an individual atom is cycled through many singlet dimers before relaxing completely, so the relaxation rate depends only on the fraction of time spent in singlet dimers, not the rate or mechanism of formation and breakup. Therefore, we simplify our treatment by ignoring three-body processes entirely. The resulting model introduces no significant inaccuracies as long as the alkali-metal density is above $\sim 10^{11}$ cm^{-3}.

To characterize the exchange process (7), we define the chemical-exchange cross section as follows; the rate at which a given member of a $^1A_2$ dimer is ejected by chemical exchange is $1/\tau_{ex} = [A]\langle \sigma_{ex} v_{AA_2} \rangle / 2$. The factor of 1/2 represents the fact that either atom may be ejected. This definition of the exchange rate is consistent with Refs. [21,24,37] but differs from Ref. [20].

Similarly, we define the dimer-reorientation cross section as follows; the rate at which the quadrupole interaction in a singlet dimer is subject to decoherence from collisions with buffer-gas species B is $1/\tau_J = [B]\langle \sigma_J v_{BA_2} \rangle$. Because of the large values of J typical of singlet dimers, this collision-induced decoherence can be thought as the reorientation of the classical dyadic $(3\hat{\mathbf{J}}\hat{\mathbf{J}} - 1)/2$ in Eq. (5).

In the following, we will often refer to a cross section for chemical exchange or reorientation. These cross sections σ are related to the relevant rate coefficient by $\langle v \rangle \sigma = \langle v \sigma(v) \rangle$, where $\langle v \rangle = \sqrt{8 k_B T / \pi \mu}$ and μ is the reduced mass of the collision pair.

TABLE II. Some important atomic parameters relevant for quadrupolar spin relaxation. The natural isotopic fraction is f, and the fraction of vapor polarization contained in nuclei of each alkali-metal species is s. The Zeeman precession frequency for each isotope is Ω_B and the nuclear spin is I.

	f	s	$\Omega_B/2\pi$ (kHz/G)	I
^{39}K	0.933	5/6	0.199	3/2
^{41}K	0.067	5/6	0.109	3/2
^{85}Rb	0.72	0.78	0.411	5/2
^{87}Rb	0.28	0.13	1.393	3/2
Cs	1.0	21/22	0.56	7/2

III. RELAXATION DUE TO SINGLET DIMERS

A. General model

Each time an alkali-metal atom becomes part of a singlet dimer, a fraction of its polarization is lost. We denote this fraction as W. Roughly speaking, therefore, the relaxation rate for atoms in an optically pumped vapor will be the rate at which the atoms are associated into singlet dimers via chemical-exchange collisions, multiplied by the fraction of the original angular momentum that is lost while in the dimer.

Put more precisely, the atomic spin-relaxation rate due to singlet molecules Γ_{sing}, defined via

$$\frac{d\langle F_z \rangle}{dt} = -\Gamma_{sing} \langle F_z \rangle, \tag{8}$$

where $\langle F_z \rangle$ is the expectation value of the z component of total angular momentum $\mathbf{F} = \mathbf{I} + \mathbf{S}$ of the free atoms, can be written as

$$\Gamma_{sing} = [^1A_2] \langle \sigma_{ex} v_{A \cdot A_2} \rangle \sum_i s_i W_i, \tag{9}$$

where the sum is over the various isotopes and s_i is the fraction of the total vapor spin angular momentum held by nucleus i and is the equivalent of the "slowing-down factor" discussed in Ref. [13]. In the low-polarization, spin-temperature limit, assuming isotopic fractions f_i, this yields

$$s_i = \frac{f_i [(I_i + 1/2)^2 - 1/4]}{1/2 + \sum f_j (I_j + 1/2)^2}. \tag{10}$$

For natural K, Rb, and Cs, the appropriate values are given in Table II.

To evaluate W, we break each atom's stay in a dimer into discrete periods of coherent spin precession. Coherence periods are brought to an end either by the atoms's ejection from the dimer, or by a buffer-gas collision, which reorients the dimer's angular momentum and changes the relaxing Hamiltonian. As shown in Appendix A, we may rewrite W_i

TABLE III. Average fractional polarization loss W_J for nuclei of spin I due to the quadrupole interaction acting for a mean time τ_c. The coherent evolution is ended either by a chemical-exchange collision (occurring at rate $1/\tau_{ex}$) or a reorienting collision (at rate $1/\tau_J$) and therefore $1/\tau_c = 1/\tau_J + 1/\tau_{ex}$. W_J is written in terms of Lorentzian functions $L(x) = 1/(1+1/x^2)$.

I	W_J
3/2	$2/5L(4\Omega_Q\tau_c/3)$
5/2	$32/105L(4\Omega_Q\tau_c/5) + 4/21L(8\Omega_Q\tau_c/5)$
7/2	$5/21L(4\Omega_Q\tau_c/7) + 4/21L(8\Omega_Q\tau_c/7) + 1/9L(12\Omega_Q\tau_c/7)$

in Eq. (9) in terms of the average fractional polarization loss during a coherence period W_{Ji}, as

$$W_i = \frac{(1+N)W_{Ji}}{1+NW_{Ji}}, \tag{11}$$

in which $N = \tau_{ex}/\tau_J$ is the mean number of reorientations per exchange collision.

Finally, we determine W_J theoretically by evolving the nuclear-density matrix under the influence of V_Q, and averaging over the exponentially distributed coherence times. We find an analytical solution, which is applicable at low magnetic field, and resort to numerical techniques for fields above a few hundred gauss. Since optical pumping is typically done at fields of less than 100 G, we expect that the analytical solution will be sufficient for most applications. As shown in Appendix B, we may write W_J in terms of Lorentzian functions $L(x) = 1/(1+1/x^2)$, where x is proportional to $\Omega_Q\tau_c$. The exact form depends on nuclear spin I, and is summarized in Table III. A discussion of the method to determine the relaxation rates at high field is given in Appendix C.

In this paper, we treat the spin relaxation of each nucleus in the dimer molecule separately. Strictly speaking, the Fermi statistics obeyed by the nuclei introduce correlations between the nuclear spins and the rotation of the molecule for homonuclear dimers that need to be accounted for. Our model ignores these correlations, and therefore potentially errs in allowing for transitions between ortho and para states of the homonuclear molecules in the vapor. However, since the total Hamiltonian, including the quadrupole interaction, is symmetric on interchange of the two nuclei, the matrix element for ortho-para transitions is zero even in a model where the Fermi statistics are ignored. The primary error in ignoring quantum statistics is in the distribution of rotational levels, an effect of little consequence at the high rotational quantum numbers (~ 60) in our experiment. Extensive analysis of quadrupolar relaxation by Happer [38], including Fermi statistics, explicitly confirms the appropriateness of approximations we have made here.

B. Limiting cases

The equations presented above are valid at all buffer-gas pressures and alkali-metal densities above 10^{11} cm^{-3}. In general, they do not have a particularly simple form and are not applicable at high magnetic fields. It is therefore instructive to examine at a few limiting cases and approximations to Eq. (9). This process also makes it clear how experimental measurements can provide values for the three parameters σ_J, σ_{ex}, and Ω_Q.

We first consider the qualitative effect of a magnetic field on the relaxation rate. As one might expect, coupling to the field must be larger than the quadrupole interaction in order to significantly affect the relaxation rate in singlet molecules. In addition, the presence of reorienting collisions adds the more stringent requirement that the nuclear precession due to the magnetic field must be large (~ 1 rad) during a coherence period for decoupling to occur. Otherwise, the (small) precessions due to the field and the quadrupole interaction simply add and do not interfere with one another. At high pressures, we show in Appendix C that, in agreement with this argument,

$$\Gamma_{sing}(B) \approx \frac{\Gamma_{sing}(0)}{1+(2\Omega_B\tau_J)^2}, \tag{12}$$

where $\hbar\Omega_B = g_I\mu_N B/I$. The change in g_I due to magnetic shielding in the singlet molecule is negligible [25].

This turns out to be quite a good approximation, even for low pressures, although the exact field dependence requires a numerical diagonalization of the complete Hamiltonian with both the magnetic-field and electric-quadrupole terms. Note that the only unknown parameter in Eq. (12) is τ_J, which makes the field dependence an excellent way to measure the molecular-reorientation rate. The more exact, numerical solution has this feature as well.

It is also instructive to consider relaxation in the limit of high and low buffer-gas pressure. In the zero-field, high-pressure limit ($\tau_J \ll \tau_{ex}, \Omega_Q^2\tau_J\tau_{ex} \ll 1$)

$$\Gamma_{sing} = \frac{[^1A_2]}{[A]} \sum_i \frac{2}{3} \frac{(2I_i-1)(2I_i+3)}{5I^2} s_i\Omega_{Qi}^2\tau_J. \tag{13}$$

The relaxation rate is inversely proportional to buffer-gas pressure, varies with alkali-metal density as $^1k_{chem}[A]$, and is independent of the chemical-exchange cross section (consistent with the assertion in Sec. I that the high-pressure relaxation rate is independent of the dimer-formation mechanism). Note that Eq. (13) depends on the interaction strength Ω_Q and reorientation rate. Once the reorientation rate has been measured by observing the magnetic-field dependence, the high-pressure relaxation rate provides a good measurement of Ω_Q.

In the low-pressure limit ($\tau_J \to \infty, \Omega_Q\tau_{ex} \gg 1$), W approaches a constant: 2/5 for a spin-(3/2) nucleus, 52/105 for spin 5/2, and 34/63 for spin 7/2. The relaxation rate therefore becomes independent of buffer-gas pressure and depends on alkali-metal density as $^1k_{chem}[A]^2$. Note, however, that the relaxation rate still depends on the chemical-exchange cross section, which makes low-pressure studies an excellent way to measure this parameter.

At pressures above about 1 Torr, we can make the approximation $N \gg 1$ (but not necessarily $NW_J \gg 1$), and the relaxation rate becomes

$$\Gamma_{sing} = \frac{[^1A_2]}{[A]} \sum_i s_i \frac{W_{Ji}/\tau_J}{1+NW_{Ji}}. \tag{14}$$

The transition between the high- and low-pressure regimes occurs when the terms in the denominator are equal—that is, at a characteristic pressure where $\tau_J = \tau_{ex} W_J$. Substituting in for W_J, and noting that $\Omega \tau_J \ll 1$, we see that the transition occurs when $\Omega_Q^2 \tau_{ex} \tau_J \approx 2/3$. This result shows that the characteristic pressure is inversely proportional to alkali density. This feature depends on all three unknown parameters and provides a good consistency check for our model.

IV. RELAXATION IN NMR EXPERIMENTS

Because of its importance in interpreting NMR experiments, in particular for determining the width of molecular NMR lines, quadrupolar relaxation has been well studied in many different contexts [39]. For alkali-metal dimers, the key features were illuminated in Ref. [20] and we review those here.

At sufficiently high pressure, relaxation is hindered by rapid reorientations of the molecular angular momentum during collisions with the buffer gas. This case is addressed for liquids in Ref. [39], Sec. VIII F(b)(3), so the derivation assumes that the reorientation is so rapid that even the molecular rotation is hindered. In gases at pressures of tens of atmospheres or less, the relaxation is averaged over the rapid rotation of the molecules. The effect of the averaging is to reduce the relaxation by a factor of 4, as explained in Sec. VIII G(a) of Ref. [39]. The high-pressure relaxation rate for nuclei in a singlet molecule (or equivalently the quadrupolar contribution to the NMR linewidth) is therefore [20,39] [see also Eq. (B11)]

$$\frac{1}{\tau_Q} = \frac{3}{160} \frac{2I+3}{I^2(2I-1)} \left(\frac{eqQ}{\hbar}\right)^2 \tau_J = \frac{2}{3} \frac{(2I+3)(2I-1)}{5I^2} \Omega_Q^2 \tau_J \approx \frac{2}{3} \Omega_Q^2 \tau_J. \tag{15}$$

Note that the relaxation rate is inversely proportional to buffer-gas pressure (through the factor τ_J) at sufficiently high pressure.

In addition to the quadrupolar contribution to the NMR linewidth, chemical-exchange collisions, and third-body breakup collisions become important at high pressures. Then the NMR linewidth becomes

$$\delta\nu = \frac{1}{\tau_Q} + [A]\langle \sigma_{ex} v_{AA_2} \rangle + [B]\langle \sigma_b v_{BA_2} \rangle, \tag{16}$$

where $\langle \sigma_b v_{BA_2} \rangle$ is the rate coefficient for breakup of the singlet molecules in collisions with third-body atoms of density $[B]$. Whereas for atomic spin relaxation the third-body breakup process can usually be ignored (see Sec. I C), for the NMR linewidth it becomes the dominant broadening mechanism at sufficiently high pressures.

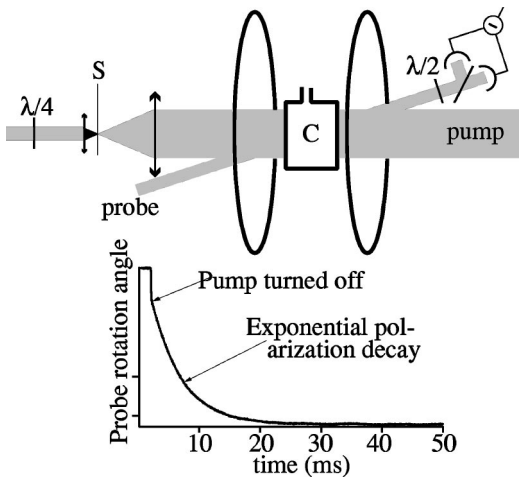

FIG. 3. Diagram of experimental apparatus with sample time-sequence data. *S*, shutter; *C*, cell with vacuum/gas manifold.

V. OVERVIEW OF EXPERIMENT

We measure the spin relaxation rate using the apparatus depicted in Fig. 3. A stainless-steel cell (1.5 in. diameter, 2.25 in. length) contains saturated alkali-metal vapor that is mixed with N_2 buffer gas. The cell has pyrex windows affixed using knife-edge gaskets in the manner of Ref. [40] and is attached to a vacuum/gas manifold that allows the N_2 pressure to be varied. The cell is contained within an oven with optical access. The oven temperature determines the alkali-metal vapor density, which is measured using Faraday rotation (as explained below) with an estimated accuracy of better than 20% [41]. The oven is placed between the pole faces of a 6-kG NMR magnet which has been modified to allow optical access along the field axis.

Our measurements are performed by optically pumping the vapor with a strong ($\sim$500 mW), circularly polarized beam from an Ar^+-pumped titanium:sapphire laser. The beam size is chosen to roughly match the fundamental diffusion mode of the cell. We then rapidly turn off the pumping light and measure vapor polarization as a function of time with a weak ($\sim$100 μW), linearly polarized probe beam. Both beams were tuned typically to 500 GHz from either the $P_{1/2}$ or the $P_{3/2}$ resonance.

The vapor-polarization measurements take advantage of polarization-induced birefringence. At large detuning, an alkali-metal vapor of density $[A]$ and polarization $P = 2\langle S_Z \rangle$ causes the probe polarization to rotate by an angle [12]

$$\phi = \frac{[A] l e^2}{6mc} \left(\frac{1}{\Delta_{3/2}} - \frac{1}{\Delta_{1/2}}\right) P \tag{17}$$

in which l is the probe path length through the vapor and $\Delta_{1/2}$, $\Delta_{3/2}$ are the detunings (in Hz) from the $P_{1/2}$ and $P_{3/2}$

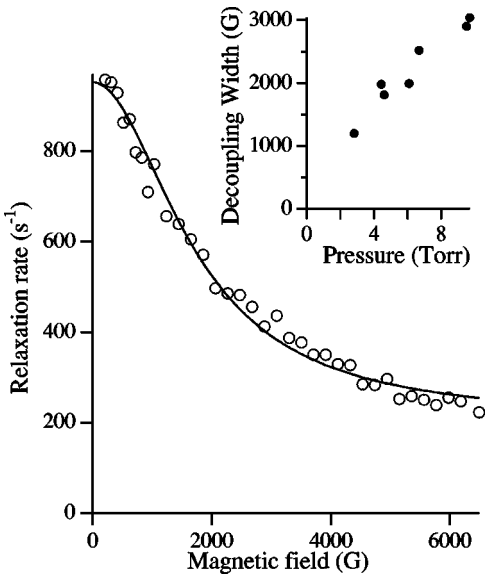

FIG. 4. Measured Rb relaxation rate as a function of magnetic field at $[\mathrm{Rb}]=1.45\times10^{15}\mathrm{cm}^{-3}$ and N_2 pressure of 6.09 Torr. The insert shows the approximately linear dependence of the field-decoupling width on buffer-gas pressure. This indicates that the duration of coherent relaxation according to Eq. (5) is cut short by collisions with the buffer gas. The solid line shows a fit to the numerically determined predictions of Eqs. (9), (10), and (11).

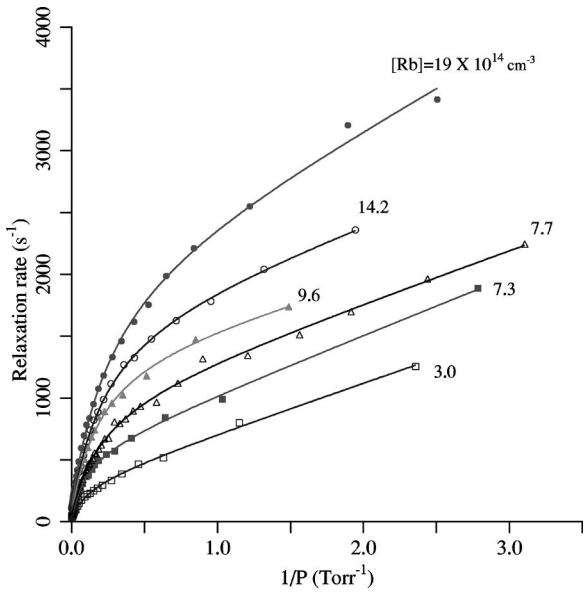

FIG. 5. Measured zero-field relaxation rate as a function of inverse buffer-gas pressure $1/P$ and Rb density. This shows how the relaxation rate in singlet dimers transitions from a region of inverse P dependence to P independence at a characteristic pressure of a few Torr. The fits are to numerical solutions of Eqs. (9), (10), and (11), and primarily constrain σ_{ex} and Ω_Q.

resonances. This is in addition to any magnetic-field-induced Faraday rotation. The rotation is detected using the balanced detector shown in Fig. 3.

A typical relaxation transient (vapor polarization vs time) is shown in the inset to Fig. 3. Note that it is usually impossible to achieve an adequate signal-to-noise ratio with one relaxation transient, so most of the data are actually an average over hundreds or thousands of transients taken with identical cell conditions. The polarization decay is always well fitted by a decaying exponential, and the inverse of the exponential time constant is the relaxation rate.

As described in Sec. III, we have used such relaxation-rate measurements to determine the cross sections σ_J, σ_{ex} and the quadrupole interaction strength Ω_Q. Figure 4 shows a sample of our measurements of Rb relaxation in N_2 as a function of magnetic field. The main part of the figure shows a typical field decoupling and the insert shows that the field width varies linearly with buffer-gas pressure in agreement with Eq. (12).

These field-dependence measurements are especially revealing because the field decoupling width depends only on the reorientation cross section. Using Eqs. (11) and (C5), we deduce that $\sigma_J=12(2)$ Å^2. Similar measurements to Fig. 4 were taken at alkali-metal densities between 2.5×10^{14} cm^{-3} and 3.0×10^{15} cm^{-3}. The field widths show no dependence on alkali-metal density at these high alkali-metal densities. The field dependence is not affected noticeably by triplet dimers [17,18] below pressures of about 25 Torr.

Figure 5 shows our measurements of zero-field Rb relaxation in N_2 in the transition region between the high- and low-pressure regimes described in Sec. II. Note that the behavior is essentially as described in Sec. III, although instead of approaching a constant at low buffer-gas pressure P, the relaxation rate continues to increase at approximately (530 s^{-1})/P (P is in Torr). We believe that this extreme low-pressure behavior is diffusion to the cell walls. If we assume that this additional low-pressure relaxation represents the decay of the lowest diffusion mode (see Ref. [13]) of the cell, we obtain a diffusion coefficient for Rb in N_2 of 0.22 cm^2/s, which is in fair agreement with the previously published value of 0.33 cm^2/s [42].

We therefore fit the measurements in Fig. 5 to a function of the form $\Gamma=\Gamma_{sing}+a_1+a_2/P$ with the additional terms representing alkali-metal–alkali-metal relaxation [17] and diffusion. These are the fits shown in Fig. 5. Note that the model accounts very well for the observed relaxation rates over a factor of 100 in pressure, and a factor of 10 in Rb density. As described in Sec. III, the combination of low- and high-pressure behavior constrains both σ_{ex} and Ω_Q and we find the best fit for $\sigma_{ex}=173(35)$ Å^2, $\Omega_Q/2\pi=300(30)$ kHz for ^{85}Rb, and $\Omega_Q/2\pi=290(29)$ kHz for ^{87}Rb. Note that since the ratio of the quadrupole moments is well known ($Q_{85}/Q_{87}=2.07$), and the field gradient q is essentially independent of isotope, we know from Eq. (6) that $\Omega_{85}/\Omega_{87}=1.035$. The two values are therefore not independent and we maintained this ratio while doing the fit.

Because of the much smaller quadrupole relaxation in K and Cs (Fig. 2), similar measurements in those alkali-metals are difficult with our current apparatus and we did not pursue them.

VI. COMPARISONS AND CONCLUSIONS

The key parameters deduced from our measurements are summarized in Table IV. Included for comparison are results

TABLE IV. Comparison of measured parameters with other experiments. The cross section for reorienting the rotational angular momentum is σ_J, the cross section for chemical exchange is σ_{ex}, and the rms quadrupole-coupling strength [defined in Eq. (6)] is Ω_Q.

Parameter	Value	Method	Ref.
$\sigma_J(Rb_2N_2)$	12 ± 2 Å^2	Spin relaxation	This work
	7.1 Å^2	Spin relaxation	[26]
σ_{ex} (Rb-Rb$_2$)	173 ± 35 Å^2	Spin relaxation	This work
	193 Å^2	Spin relaxation	[26]
	193 Å^2	Theory	This work
$\sqrt{\Omega_Q^2}/2\pi$ (^{85}Rb)	300 ± 30 kHz	Spin relaxation	This work
	250 kHz	Spin relaxation	[26]
$\Omega_Q/2\pi$ (^{85}Rb)	>103 kHz	Molecular beam	[33]

from previous experiments, which we now discuss

The electric-quadrupole interaction has been studied previously and values for σ_{ex} and σ_J inferred by observing the dependence of NMR linewidths on experimental conditions. The first such experiment, by Gupta *et al.* [20], quotes approximate values for Cs in Ne that are similar to ours in order of magnitude. Subsequent work on Na [22,21], K [23], and Cs [21] gives similar values as well. None of these works used Rb and are therefore not directly comparable to this experiment.

Atom-dimer exchange processes have also been studied using colliding atomic and molecular beams (usually of unlike species) [43], and yield cross sections similar to our measurements. We have performed classical-trajectory Monte Carlo modeling of atom-dimer exchange collisions using the trimer potential of Ref. [44] scaled to reflect recent dimer binding-energy data (see Sec. I). Because of the large angular momenta typical of these collisions, a semiclassical calculation should be sufficient, and the reliability of these results is probably limited by the quality of the trimer Born-Oppenheimer potential. We predict a chemical-exchange cross section of 180 Å^2 in K, 193 Å^2 in Rb, and 210 Å^2 in Cs. This work compares favorably to our measurements as well. See Ref. [45] for a similar calculation.

A very direct comparison can be made between the experiments described here and the previously unpublished results of the Erickson [26], shown also in Table IV. Erickson's results for the chemical-exchange cross section agree well with the results of Kadlecek, especially considering that absolute Rb density measurements are required. Similarly, the deduced values of Ω_Q are in good agreement. On the other hand, the deduced values for σ_J, which are determined mainly from the magnetic-decoupling widths, disagree by about 40%, a surprisingly large value. We have not been able to reconcile this discrepency.

There has also been one previous measurement of Ω_Q. This measurement, made by Logan *et al.* in 1952 [33], used molecular-beam methods to measure the quadrupole energy splittings directly. Their quoted values [translated using Eq. (6)] are $\Omega_Q/2\pi=103$ kHz, about a factor of 3 smaller than what we have deduced in this work.

This discrepancy may be partially resolved by noting, as has been recognized before (see Ref. [33] and references therein), that the interaction strength Ω_Q varies with the molecular rovibrational state. The result of Logan *et al.* must be interpreted as the statistically most likely value of the interaction strength, whereas the spin-relaxation experiment measures the root-mean-square value. We also note that due to certain experimental artifacts (discussed in Ref. [33]), the Logan *et al.* results were intended only as a lower bound on Ω_Q. Rb was singled out as a case where the experimental broadening was particularly severe. Thus we do not feel that our experimental results are necessarily in conflict with the Logan *et al.* results.

In conclusion, we have measured spin relaxation in alkali-metal singlet dimers, and have developed a model that accurately explains these results. This model allows prediction of relaxation rates in other alkali-metal and buffer-gas species, and at all alkali-metal densities, buffer-gas pressures, and magnetic-field strengths. In addition, comparison with experimental measurements gives interesting quantitative information about microscopic dynamical processes taking place in the vapor.

ACKNOWLEDGMENTS

This work was supported by the National Science Foundation. We thank W. Happer for his original suggestion to investigate the magnetic decoupling, and careful reading and critique of the manuscript.

APPENDIX A: RELAXATION FRACTION DURING A DIMER LIFETIME

This appendix describes our calculation of the average fractional polarization loss W during the period an alkali-metal atom is bound in a singlet dimer. The polarization loss is caused by the electirc-quadrupole interaction, although coherent relaxation is typically interrupted many times by buffer-gas collisions that reorient the direction of the dimer's angular momentum. The task in this appendix is therefore to write W in terms of the average polarization loss during a coherence period, which we refer to as W_J, and which we derive in Appendix B.

If an atom undergoes N coherence periods before exiting a molecule, then the fraction of polarization remaining is $[1-(1-W_J)^N]$. Note that because decoherence events are randomly distributed in time, setting a fixed value for N does not change the distribution of coherence period lengths that will be used for calculating W_J. Note also that in order to assume that each W_J is the same, we must assume that the spin-temperature density matrix remains a good description of the actual density matrix at the end of each coherence period. We shall see in Appendix B that this is the case at zero magnetic field.

Now, if $P(N)$ is the probability of getting N coherence periods before leaving the dimer, the average fractional polarization loss W is

$$W=\sum_{N=1}^{\infty} P(N)[1-(1-W_J)^N]=1-\sum_{N=1}^{\infty} P(N)(1-W_J)^N. \tag{A1}$$

To evaluate $P(N)$, we simply integrate over all possible molecular lifetimes and coherence times while maintaining N coherence periods. Thus one can show that

$$\begin{aligned}P(N)&=\int_0^\infty\frac{dt_1}{\tau_{ex}}e^{-t_1/\tau_{ex}}\int_0^{t_1}\frac{dt_2}{\tau_J}e^{-t_2/\tau_J}\cdots\\&\quad\times\int_0^{t_1-t_2-\cdots-t_{N-1}}e^{-t_N/\tau_J}e^{-(t_x-t_2-\cdots-t_N)\tau_J}\frac{dt_N}{\tau_J}\\&=\frac{1}{\tau_{ex}\tau_J^{N-1}}\int_0^\infty dt_1e^{-t_1/\tau_c}\int_0^{t_1}dt_2\cdots\int_0^{t_1-\cdots-t_{N-1}}dt_N\\&=1/(\tau_{ex}\tau_J^{N-1})\int_0^\infty dt_1e^{-t_1/\tau_c}\int_0^{t_{ex}}dt_2\int_0^{t_2}dt_3\cdots\\&\quad\times\int_0^{t_{N-1}}dt_N\\&=1/(\tau_{ex}\tau_J^{N-1})\int_0^\infty dt_1e^{-t_1/\tau_c}\frac{t_1^{(N-1)}}{(N-1)!}=\frac{\tau_{ex}^{N-1}\tau_J}{(\tau_{ex}+\tau_J)^N},\end{aligned}\tag{A2}$$

and therefore that

$$W=1-\frac{\tau_J}{\tau_{ex}}\sum_{N=1}^{\infty}\left[\frac{\tau_{ex}(1-W_J)}{\tau_{ex}+\tau_J}\right]^N=\frac{(1+\langle N\rangle)W_J}{1+\langle N\rangle W_J}\tag{A3}$$

in which $\langle N\rangle=\tau_{ex}/\tau_J$ is the average number of reorientations before an exchange.

APPENDIX B: RELAXATION FRACTION DURING A COHERENCE TIME; $B=0$

This appendix details our calculation of coherent nuclear relaxation of a single nucleus contained in a singlet molecule. We show that, for small applied magnetic fields, the fraction of polarization lost during a period τ_c of coherent evolution can be written as a Lorentzian function of $1/\tau_c$ for nuclear spin $I\leqslant 3/2$, or as a sum of Lorentzians for higher spin.

Coherent evolution is interrupted by molecular reorientation and chemical exchange, which are both random collisional events. We therefore expect that the nuclear spin will be allowed to evolve coherently for a duration τ distributed as

$$P(\tau)=\frac{1}{\tau_c}e^{-\tau/\tau_c}\tag{B1}$$

in which $1/\tau_c=1/\tau_J+1/\tau_{ex}$. The density matrix after a period of coherent evolution should therefore be averaged over period durations and a random distribution of molecular orientations $\hat{\mathbf{J}}$ as

$$\rho_F=\Theta_{\mathrm{Eu}}\int_0^\infty\frac{d\tau}{\tau_c}e^{-\tau/\tau_c}e^{-iH\tau}\rho_0e^{iH\tau}.\tag{B2}$$

The Hamiltonian includes both the quadrupole interaction and a Zeeman interaction with the applied laboratory magnetic field. Θ_{Eu} denotes an average over Euler angles for $\hat{\mathbf{J}}$. We assume that evolution begins with an axially symmetric density-matrix distribution

$$\rho_0=\frac{1}{2I+1}\left[1+\frac{3\langle I_z\rangle I_z}{I(I+1)}\right],\tag{B3}$$

where z denotes the direction of the laboratory magnetic field, and we have assumed that the higher moments of the density matrix can be neglected, as is valid for high-spin temperatures.

It is convenient to evaluate Eq. (B2) in the basis of eigenstates $|m'\}$ of H with eigenvalues $E_{m'}$,

$$\begin{aligned}\{m'|\rho_F|n'\}&=\Theta_{\mathrm{Eu}}\int_0^\infty\frac{d\tau}{\tau_c}\exp[-\tau/\tau_c-i\omega_{m'n'}\tau]\{m'|\rho_0|n'\}\\&=\Theta_{\mathrm{Eu}}\frac{\{m'|\rho_0|n'\}}{(1+i\omega_{m'n'}\tau_c)},\end{aligned}\tag{B4}$$

where $\hbar\omega_{m'n'}=E_{m'}-E_{n'}$. Transforming back to the laboratory basis,

$$\rho_F=\Theta_{\mathrm{Eu}}\sum_{m'n'}\frac{|m'\}\{m'|\rho_0|n'\}\{n'|}{1+i\omega_{m'n'}\tau_c}.\tag{B5}$$

The derivation thus far is independent of the form of the interaction and may be solved, in general, numerically. In the rest of this appendix we neglect the magnetic field. In this case, it is clear that the transformation that diagonalizes the quadrupole interaction V_Q is the rotation to the primed system $\hat{\mathbf{z}}'=\hat{\mathbf{J}}$. The Bohr frequencies are

$$\omega_{m'n'}=\frac{\Omega_Q}{I}(m'^2-n'^2).\tag{B6}$$

The diagonal density-matrix elements in the laboratory basis are

$$\rho_{Fmm}=\Theta_{\mathrm{Eu}}\sum_{m'n'n}\frac{\rho_{nn}\langle m|m'\}\{m'|n\rangle\langle n|n'\}\{n'|m\rangle}{1+i\omega_{m'n'}\tau_c}.\tag{B7}$$

The bra-ket inner products can be written in terms of Wigner D functions, and reduced by the Clebsch-Gordan series [46] to ease the angular integration,

$$\begin{aligned}\rho_{Fmm}&=\sum_{m'n'n}\frac{\rho_{nn}}{1+i\omega_{m'n'}\tau_c}\Theta_{\mathrm{Eu}}(D^I_{mm'}D^{I*}_{nm'}D^I_{nn'}D^{I*}_{mn'})\\&=\sum_{jnn'm'}\frac{\rho_{nn}(-)^{2I-j}}{1+i\omega_{m'n'}\tau_c}\frac{[C^{jm+n}_{ImIn}]^2[C^{jm'+n'}_{Im'In'}]^2}{2j+1}.\end{aligned}$$

Note that $\Sigma_n n[C^{jm+n}_{ImIn}]^2$ is proportional to m for all j,m. This ensures that in the low-polarization limit, if the density matrix begins in a spin-temperature distribution, it will remain a spin-temperature distribution (albeit at a different temperature) to start the next period of coherent evolution.

We may now write the fractional polarization loss during a coherence time as

$$W_J(\tau_c)=1-\left(\sum_m m\rho_{Fmm}\right)\Big/\left(\sum_m m\rho_{0mm}\right). \quad \text{(B8)}$$

In the low-polarization limit [Eq. (B3)], and using Eqs. 12.1(8) and 8.7(31) of Ref. [46], this becomes

$$W_J(\tau_c)=\sum_{m,n=-I}^{I}\frac{\omega_{mn}^2\tau_c^2}{1+\omega_{mn}^2\tau_c^2}\sum_{j=0}^{2I}[C^{jm+n}_{ImIn}]^2\begin{Bmatrix}1 & I & I\\ j & I & I\end{Bmatrix}$$

$$=\sum_{m,n=-I}^{I}\frac{\omega_{mn}^2\tau_c^2}{1+\omega_{mn}^2\tau_c^2}\frac{[C^{Im}_{1n-mIn}]^2}{2I+1}. \quad \text{(B9)}$$

Thus W_J is a simple Lorentzian function of $1/\tau_c$ for nuclear spin $I\leqslant 3/2$, or a sum of Lorentzians for higher spin. We find it convenient to write the terms out explicitly for half-integer spins as

$$W_J(\tau_c)=\sum_{l=1} c_l\frac{(2l\Omega_Q\tau_c/I)^2}{1+(2l\Omega_Q\tau_c/I)^2}, \quad \text{(B10)}$$

where the coefficients c_l are given explicitly in Table III.

Note that for short coherence times, Eq. (B9) reduces to

$$W_J(\tau_c)=\frac{2}{3}\frac{(2I-1)(2I+3)}{5I^2}\Omega_Q^2\tau_c^2, \quad \text{(B11)}$$

in agreement with Ref. [39]. In the limit of long coherence times (low pressure),

$$W_J=\begin{cases}\dfrac{2}{3}, & I=1,2,3\ldots\\ \dfrac{2}{3}-\dfrac{1+2I}{4I(1+I)}, & I=3/2,5/2\cdots\end{cases} \quad \text{(B12)}$$

W_J is less than 2/3 for half-integers because the $m=1/2$ and $m=-1/2$ states are degenerate and therefore do not contribute to the relaxation.

APPENDIX C: MAGNETIC-FIELD DEPENDENCE OF W_J

The previous appendix gave analytical results for the singlet relaxation at zero magnetic field. When the magnetic field cannot be neglected, the eigenstates of the Hamiltonian are not simple enough to allow for analytic formulas to be calculated for W_J, except in extreme cases. In particular, in order to analyze the data of Fig. 4, we find it necessary to find W_J numerically.

In the presence of a magnetic field, the Hamiltonian for one of the nuclei in the molecule becomes

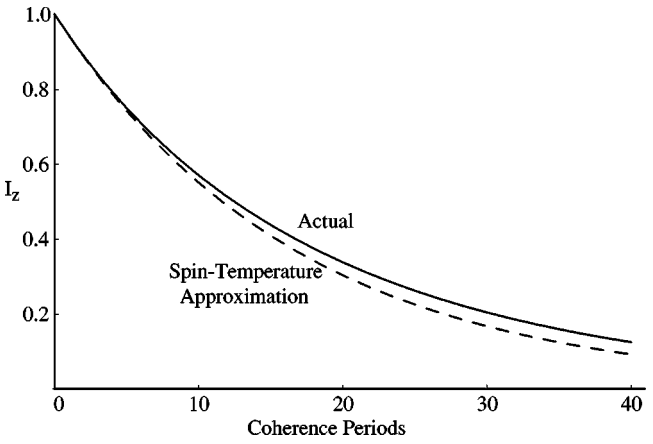

FIG. 6. Test of the spin-temperature assumption for reorientation of a spin-(5/2) nucleus at nonzero magnetic field ($\Omega_B\tau=2.0$).

$$H=V_Q-\frac{g_I\mu_N BI_z}{I}, \quad \text{(C1)}$$

where the magnetic field is presumed to lie along the z axis. If we denote the eigenstates of H as $|p\}$ with energies E_p, the time-evolved density matrix becomes, in analogy to Eq. (B5),

$$\rho_F=\Theta_{\mathrm{Eu}}\sum_{pq}\frac{|p\}\{p|\rho_0|q\}\{q|}{1+i\omega pq\tau_c}. \quad \text{(C2)}$$

The fraction of spin lost during a coherent precession is

$$W_J=\frac{\langle I_z\rangle_0-\langle I_z\rangle_F}{\langle I_z\rangle_0} \quad \text{(C3)}$$

$$=\Theta_{\mathrm{Eu}}\sum_{pq}\frac{\{p|I_z|q\}\{q|\rho_0|p\}\omega_{pq}^2\tau_c^2}{1+\omega_{pq}^2\tau_c^2}, \quad \text{(C4)}$$

which, using Eq. (B3), becomes

$$W_J=\Theta_{\mathrm{Eu}}\sum_{pq}\frac{3\{p|I_z|q\}\{q|I_z|p\}}{I(I+1)(2I+1)}\frac{\omega_{pq}^2\tau_c^2}{1+\omega_{pq}^2\tau_c^2}. \quad \text{(C5)}$$

Thus we numerically solve for W_J by finding the numerical eigenstates $|q\}$ and energies E_q, finding the matrix elements of I_z in that basis, and apply the τ_c-dependent factors.

In contrast to the zero-field case, we do not necessarily find that the density matrix can still be described by a spin temperature at the end of a coherence period. However, Monte Carlo simulations suggest that the spin-temperature assumption remains reasonable at moderate field strengths. An example of the difference between the spin-temperature approximation and keeping the full density matrix is shown in Figure 6.

When the Zeeman interaction strength is much greater than the electric-quadrupole interaction, we can use perturbation theory to evaluate Eq. (C5). To first order in V_Q, the perturbed states are

$$|q\} = |q\rangle + \sum_k \frac{\langle k|V_Q|q\rangle}{\hbar\omega_{qk}} \tag{C6}$$

and W_J becomes, to second order in V_Q,

$$W_J = \frac{3\tau_c^2}{I(I+1)(2I+1)\hbar^2}\Theta_{\mathrm{Eu}}\sum_{pq}\frac{(p-q)^2|\langle p|V_Q|q\rangle|^2}{1+\omega_{0pq}^2\tau_c^2}, \tag{C7}$$

where $\hbar\omega_{0pq} = -(p-q)g_I\mu_N B/I = (p-q)\hbar\Omega_B$. This can be simplified in a manner similar to Appendix B to obtain

$$W_J = \frac{2}{3}\frac{(2I-1)(2I+3)}{5I^2}\Omega_Q^2\tau_c^2\sum_{r=1}^{2}\frac{r^2/5}{1+r^2\Omega_B^2\tau_c^2}, \tag{C8}$$

which in the short-coherence-time limit again simplifies to Eq. (B11). The magnetic-field dependence is the sum of two Lorentzians whose widths depend on the coherence time. The validity of this formula requires $g_i\mu_n B/I \gg 3\hbar\Omega_Q$, or $B \gg 1500$ G, for ^{85}Rb. It will also work well when the pressure-broadened field width exceeds this value, which happens for ^{85}Rb at pressures greater than a few Torr. For most spin-exchange optical-pumping conditions, Eq. (C8) is an excellent and convenient approximation for estimating the effects of quadrupole relaxation. Much of our data for this experiment was however taken outside the region of applicability of Eq. (C8), so we have fit our data to the full numerical solution rather than the high-field approximation.

It is straightforward to obtain an analogous expression for relaxation due to the nuclear spin-rotation interaction,

$$W_J = \frac{2}{3}\frac{(c'J\tau_c)^2}{1+\Omega_B^2\tau_c^2}. \tag{C9}$$

Using the information from Table I, we estimate that the spin-rotation coupling makes at most a 5% difference for Rb but is much more important for Cs and K.

[1] M. A. Bouchiat, T. R. Carver, and C. M. Varnum, Phys. Rev. Lett. **5**, 373 (1960).
[2] T. Walker and W. Happer, Rev. Mod. Phys. **69**, 629 (1997).
[3] M. S. Albert *et al.*, Nature (London) **370**, 199 (1994).
[4] T. E. Chupp, R. J. Hoare, R. L. Walsworth, and B. Wu, Phys. Rev. Lett. **72**, 2363 (1994).
[5] G. Jones *et al.*, Nucl. Instrum. Methods Phys. Res. A **440**, 772 (2000).
[6] P. Anthony *et al.*, Phys. Rev. Lett. **71**, 959 (1993).
[7] Z. Wu, W. Happer, M. Kitano, and J. Daniels, Phys. Rev. A **42**, 2774 (1990).
[8] D. Raferty *et al.*, Phys. Rev. Lett. **66**, 584 (1991).
[9] H. Jansch *et al.*, Chem. Phys. Lett. **296**, 146 (1998).
[10] D. Schmidt J. Magn. Reson. **129**, 184 (1997).
[11] A. Ben-AmarBaranga; *et al.*, Phys. Rev. A **58**, 2282 (1998).
[12] S. Kadlecek, Ph.D. thesis, University of Wisconsin, Madison, 2000.
[13] W. Happer, Rev. Mod. Phys. **44**, 169 (1972).
[14] N. D. Bhaskar, J. Pietras, J. Camparo, and W. Happer, Phys. Rev. Lett. **44**, 930 (1980).
[15] R. J. Knize, Phys. Rev. A **40**, 6219 (1989).
[16] M. E. Wagshul and T. E. Chupp, Phys. Rev. A **49**, 3854 (1994).
[17] S. Kadlecek, L. W. Anderson, and T. Walker, Phys. Rev. Lett. **80**, 5512 (1998).
[18] C. J. Erickson *et al.*, Phys. Rev. Lett. **85**, 4237 (2000).
[19] M. A. Bouchiat, J. Brossel, and L. C. Pottier, J. Chem. Phys. **56**, 3703 (1972).
[20] R. Gupta, W. Happer, G. Moe, and W. Park, Phys. Rev. Lett. **32**, 574 (1974).
[21] M. Kompitsas and H. G. Weber, Chem. Phys. Lett. **35**, 277 (1975).
[22] R. Huber and H. G. Weber, Chem. Phys. **37**, 173 (1979).
[23] W. Kamke, Phys. Lett. **55A**, 15 (1975).
[24] H. Weber, Z. Phys. A **284**, 145 (1978).
[25] R. Huber *et al.*, Z. Phys. A **296**, 95 (1980).
[26] C. Erickson, Ph.D. thesis, Princeton University, 1999.
[27] M. Krauss and W. J. Stevens, J. Chem. Phys. **93**, 4236 (1990).
[28] M. Elbs *et al.*, Phys. Rev. A **59**, 3665 (1999).
[29] C. Amiot, J. Mol. Spectrosc. **147**, 370 (1991).
[30] C. C. Tsai *et al.*, Phys. Rev. Lett. **79**, 1245 (1997).
[31] M. Marinescu, H. R. Sadeghpour, and A. Dalgarno, Phys. Rev. A **49**, 982 (1994).
[32] H. M. J. M. Boesten, C. C. Tsai, B. J. Verhaar, and D. J. Heinzen, Phys. Rev. Lett. **77**, 5194 (1996).
[33] R. A. Logan, R. E. Coté, and P. Kusch, Phys. Rev. **86**, 280 (1952).
[34] C. H. Townes and A. L. Schawlow, *Microwave Spectroscopy* (Dover, New York, 1975).
[35] P. E. V. Esbroeck *et al.*, Phys. Rev. A **32**, 2595 (1985).
[36] H.-J. Glas and H. G. Weber, Z. Phys. A **284**, 253 (1978).
[37] J. C. Whitehead and R. Grice, Faraday Discuss. Chem. Soc. **55**, 320 (1973).
[38] W. Happer (unpublished).
[39] A. Abragam, *Principles of Nuclear Magnetism* (Oxford University Press, Oxford, 1961).
[40] A. Noble and M. Kasevich, Rev. Sci. Instrum. **65**, 3042 (1994).
[41] E. Vliegen, S. Kadlecek, L. W. Anderson, and T. G. Walker, Nucl. Instrum. Methods Phys. Res. A **460**, 444 (2001).
[42] R. J. McNeal, J. Chem. Phys. **37**, 2726 (1962).
[43] D. J. Mascord, H. W. Cruse, and R. Grice, Mol. Phys. **32**, 131 (1976).
[44] J. L. Martins, R. Car, and J. Buttet, J. Chem. Phys. **78**, 5646 (1983).
[45] J. C. Whitehead, Mol. Phys. **29**, 177 (1975).
[46] D. A. Varshalovich, A. N. Moskalev, and V. K. Khersonskii, *Quantum Theory of Angular Momentum* (World Scientific, Singapore, 1988).